PARAMAGENTISM IN PRIMORDIAL UNIVERSE

Andrew Steinmetz[ID], Cheng Tao Yang[ID], and Johann Rafelski[ID]

Department of Physics, The University of Arizona, Tucson, AZ 85721, USA

June 25, 2023

ABSTRACT

We explore primordial universe magnetization of the ultra dense electron-positron e^+e^- plasma in the temperature range $200\,\mathrm{keV} > T > 20\,\mathrm{keV}$ driven by spin paramagnetism. The e^+e^- pair density prior to Big Bang Nucleosynthesis (BBN) was more than 10^8 greater than the baryon density. Pairs fully disappear only below $T = 20\,\mathrm{keV}$. ANDREW: Everywhere in the text we restrict ourselves to 200 keV as the maximum temperature to discuss but all our plots go to 2000 keV. I suggest we either: (a) restrict our plots, (b) provide an in-text explanation for the distinction (c) expand text to cover up to 2000 keV (d) or some combination thereof.

Keywords early universe cosmology · magnetization · electron-positron plasma · intergalactic magnetic fields

1 Introduction

Considering the ubiquity of magnetic fields [1, 2] in the universe, we search for a primordial mechanism which could produce the diversity of magnetism observed today. Macroscopic domains of magnetic fields have been found around compact objects (stars, planets, etc...); between stars; within galaxies; between galaxies in clusters; and surprisingly in deep extra-galactic void spaces. The conventional elaboration of the origins for cosmic primordial magnetic fields (PMF) are detailed in [3, 4, 5].

Intergalactic magnetic field (IGMF) are difficult to measure and difficult to explain. In this work, IGFM will refer to experimentally observed intergalactic fields of any origin while PMF refers to fields generated via primordial (early universe) processes. The bounds for IGMF at a length scale of $1\,\mathrm{Mpc}$ are today [6, 7, 8, 9, 10]

$$10^{-8}\,\mathrm{G} > \mathcal{B}_{\mathrm{IGFM}} > 10^{-16}\,\mathrm{G}\,. \tag{1}$$

Faraday rotation from distant radio active galaxy nuclei (AGN) [11] suggest that neither dynamo nor astrophysical processes would sufficiently account for the presence of magnetic fields in the universe today if the IGMF strength was around the upper bound of $\mathcal{B}_{\mathrm{IGMF}} \simeq 30 - 60\,\mathrm{nG}$ as found in Ref. [10]. Such strong magnetic fields would then require that at least some portion of the IGMF arise from primordial sources that predate the formation of stars.

We investigate the hypothesis that the observed IGMF are primordial in nature, predating even the recombination epoch. Specifically, we explore the role of the relatively large electron-positron (e^+e^-) pair abundance which only disappears well after Big Bang nucleosynthesis (BBN). Electrons and positrons, having the largest magnetic moments in nature, are likely to have been magnetized in the pre-BBN early universe due to spin orientation. The rapid 10^8 drop in e^+e^- abundance within the narrow temperature range $200\,\mathrm{keV} > T > 20\,\mathrm{keV}$ shown in Fig. 1 should then be capable of inducing dynamical currents preserving magnetic flux in the emerging p, α, e^- plasma.

Large pre-recombination primordial fields could therefore lead to early universe baryon inhomogeneities which in turn would produce anisotropies in the cosmic microwave background (CMB) [12, 13]. Jedamzik and Pogosian [14] propose further that the presence of $\mathcal{B}_{\mathrm{PMF}} \simeq 0.1\,\mathrm{nG}$ could be sufficient to explain the Hubble tension. We consider an entirely novel hypothesis that the primordial magnetization of the universe is driven by spin paramagnetism originating in the relatively dense electron-positron e^+e^- plasma which reached about 100 million pairs per baryon at the pre-BBN temperature $T = 200\,\mathrm{keV}$ (see: Fig. 1). These results were obtained using charge neutrality and the baryon to photon content (entropy) of the universe [15].
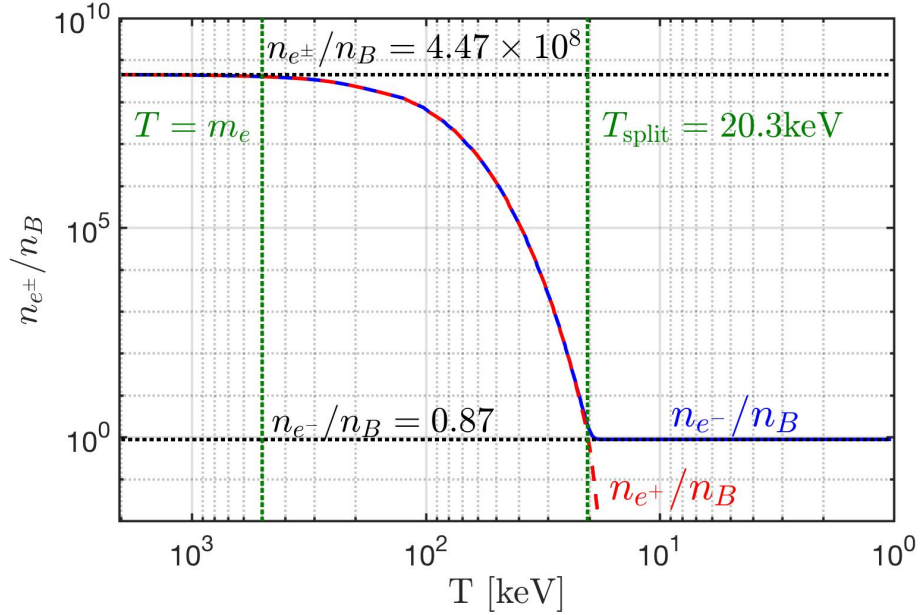
Figure 1: Electron e^- and positron e^+ to baryon ratio $n_{e^\pm}/n_B$ as a function of photon temperature in the universe. See text for further details.

The electron-to-baryon ratio n_{e^-}/n_B is shown in Fig. 1 as the solid blue line which overlaps the positron-to-baryon ratio n_{e^+}/n_B, represented by the dashed red line, until the temperature drops below $T_{\text{split}} = 20.3\,\text{keV}$ as the abundances of the two species diverge from one another. The two vertical dashed green lines denote temperatures $T = m_e \simeq 511\,\text{keV}$ and $T_{\text{split}} = 20.3\,\text{keV}$. It is customary to show time as increasing from left to right which corresponds to a decreasing temperature. All figures in this paper will plot temperature as the x-axis scale. The two horizontal black dashed lines denote the relativistic $T \gg m_e$ abundance of $n_{e^\pm}/n_B = 4.47 \times 10^8$ and post-annihilation abundance of $n_{e^-}/n_B = 0.87$. The deviation from unity in the post-annihilation abundance reflects the presence of bound neutrons in the baryon content. Above temperature $T \simeq 85\,\text{keV}$, the $e^+ e^-$ primordial plasma density exceeded that of the Sun's core density $n_e \simeq 6 \times 10^{26}\,\text{cm}^{-3}$ [16].

Our analysis of the relativistic fermion partition function focuses on the spin contribution to magnetization. At $T \simeq 200\,\text{keV}$, due to very high $e^+ e^-$ pair densities, we believe that spin paramagnetism is dominant over Landau orbital diamagnetism. We show that magnetization is nonzero even for a nearly symmetric particle-antiparticle gas as well as account for the matter-antimatter asymmetry present in the universe. We further demonstrate that magnetization can spontaneously increase in strength near the IGMF upper limit seen in Eq. (1). This is assisted by the fact that antiparticles (e^+) have the opposite sign of charge, and thus magnetic moment, compared to particles (e^-). Therefore in an $e^+ e^-$ pair plasma, net magnetization can be associated with opposite spin orientations for particles and antiparticles without the accompaniment of a net angular momentum in the volume considered. This is of course very different from the the matter dominated universe arising below $T \simeq 20\,\text{keV}$ which includes the current epoch.

2 Electron-positron abundance

As the universe cooled below temperature $T = m_e$ (the electron mass), the thermal electron and positron comoving density of $n_{e^\pm}/n_B = 4.47 \times 10^8$ depleted falling over eight orders of magnitude. At $T_{\text{split}} = 20.3\,\text{keV}$, the charged lepton asymmetry (mirrored by baryon asymmetry and enforced by charge neutrality) became evident as the surviving excess electrons persisted while positrons vanished entirely from the particle inventory of the universe. Conversion of the dense $e^+ e^-$ pair plasma into photons reheated the photon background [17] separating the photon and neutrino temperatures. The $e^+ e^-$ annihilation and photon reheating period lasted no longer than an afternoon lunch break. Because of charge neutrality, the post-annihilation comoving ratio $n_{e^-}/n_B = 0.87$ [15] is slightly offset from unity in Fig. 1 by the presence of bound neutrons in α particles and other neutron containing light elements produced during BBN epoch.

To obtain a quantitative description of the above evolution, we study the bulk properties of the relativistic charged/magnetic gasses in a nearly homogeneous and isotropic primordial universe via the thermal Fermi-Dirac or Bose distributions. For matter ($\sigma = +1$) and antimatter ($\sigma = -1$) particles, a nonzero chemical potential $\mu_\sigma = \sigma\mu$ is caused by an imbalance of matter and antimatter. While the primordial electron-positron plasma era was overall charge neutral, there was a small asymmetry in the charged leptons from baryon asymmetry [18, 19] in the universe. Consideration of reactions such as $e^+ e^- \leftrightarrow \gamma\gamma$ constrains the chemical potentials of electrons and positrons [20] as

$$\mu \equiv \mu_{e^-} = -\mu_{e^+}, \qquad \lambda \equiv \lambda_{e^-} = \lambda_{e^+}^{-1} = \exp\frac{\mu}{T}, \tag{2}$$

where λ is the fugacity of the system.

During the e^+e^- plasma epoch, the density changed dramatically over time (see: Fig. 1) changing the chemical potential in turn. We can then parameterize the chemical potential of the e^+e^- plasma as a function of temperature $\mu \to \mu(T)$ via the charge neutrality of the universe which implies

$$n_p = n_{e^-} - n_{e^+} = \frac{1}{V}\lambda\frac{\partial}{\partial\lambda}\ln\mathcal{Z}_{e^+e^-}. \tag{3}$$

In Eq. (3), n_p is the observed total number density of protons in all baryon species. The parameter V relays the proper volume under consideration and $\ln\mathcal{Z}_{e^+e^-}$ is the partition function for the electron-positron gas. The chemical potential defined in Eq. (2) is obtained from the requirement that the positive charge of baryons (protons, α particles, light nuclei produced after BBN) is exactly and locally compensated by a tiny net excess of electrons over positrons.

The abundance of baryons is itself fixed by the known abundance relative to photons [21] and we employed the contemporary recommended value $n_B/n_\gamma = 6.09 \times 10^{-10}$. The resulting chemical potential needs to be evaluated carefully to obtain the behavior near to $T_{\text{split}} = 20.3$ keV where the relatively small value of chemical potential μ rises rises rapidly so that positrons vanish from the particle inventory of the universe while nearly one electron per baryon remains. The detailed solution of this problem is found in Refs. [18, 15] leading to the results shown in Fig. 1. These results are obtained allowing for Fermi-Dirac and Bose statistics, however it is often numerically sufficient to consider the Boltzmann distribution limit.

In the presence of a magnetic field $\mathcal{B}$ there is some modification of the usual relativistic fermion partition function which is now given by

$$\ln\mathcal{Z}_{e^+e^-} = \frac{e\mathcal{B}V}{(2\pi)^2}\sum_\sigma^\pm\sum_s^\pm\sum_{n=0}^\infty\int_{-\infty}^\infty dp_z\left[\ln\left(1 + \lambda_\sigma\xi_s e^{-E_n^s/T}\right)\right], \qquad \Upsilon_\sigma^s = \lambda_\sigma\xi_s = \exp\frac{\mu_\sigma + \eta_s}{T}, \tag{4}$$

with electric charge $e \equiv q_{e^+} = -q_{e^-}$. The index σ in Eq. (4) is a sum over electron and positron states while s is a sum over polarizations. Since we are interested in small asymmetries (e.g. baryon excess over antibaryons, one spin polarization over another) we introduce the generalized particle fugacity Υ_σ^s as the product of:

    a. Chemical fugacity λ_σ

    b. Spin fugacity ξ_s

The chemical fugacity λ_σ (defined in Eq. (2) above) describes deformation of the Fermi-Dirac distribution due to nonzero chemical potential μ. An imbalance in electrons and positrons leads as discussed earlier to a nonzero particle chemical potential $\mu \neq 0$. We then introduce a novel spin fugacity ξ_s and spin potential $\eta_s = s\eta$. We propose the spin potential follows analogous expressions as seen in Eq. (2) obeying

$$\eta \equiv \eta_+ = -\eta_-, \qquad \xi \equiv \xi_+ = \xi_-^{-1} = \exp\frac{\eta}{T}. \tag{5}$$

An imbalance in spin polarization within a region of volume V results in a nonzero spin potential $\eta \neq 0$. Conveniently since antiparticles have opposite sign of charge and magnetic moment, the same magnetic moment is associated with opposite spin orientation for particles and antiparticles independent of degree of spin-magnetization. A completely particle-antiparticle symmetric magnetized plasma will have therefore zero total spin angular momentum and zero spin potential $\eta = 0$. This is of course very different from the situation today of a matter dominated universe.

3 Primordial paramagnetism

As the universe undergoes isotropic expansion, the temperature decreases as

$$T(t) = T_0\frac{a_0}{a(t)} \to T(z) = T_0(1+z), \tag{6}$$

where $a(t)$ is the scale factor defined by the FLRW metric [22] and z is the redshift. The comoving temperature T_0 is given by the present day temperature of the CMB, with contemporary scale factor $a_0 = 1$. Within a homogeneous magnetic domain, the magnetic field varies [4] over cosmic expansion as

$$\mathcal{B}(t) = \mathcal{B}_0 \frac{a_0^2}{a^2(t)} \to \mathcal{B}(z) = \mathcal{B}_0 \left(1 + z\right)^2 , \tag{7}$$

where $\mathcal{B}_0$ is the comoving value of the magnetic field obtained from the contemporary value of the magnetic field today given in Eq. (1). Non-primordial magnetic fields (which are generated through other mechanisms such as dynamo or astrophysical sources) do not follow this scaling [11]. The presence of matter and late universe structure formation also contaminates the primordial field evolution in Eq. (7). It is only in deep intergalactic space where primordial fields remain preserved and comoving over cosmic time.

From Eq. (6) and Eq. (7) emerges a natural ratio of interest here which is conserved over cosmic expansion

$$b \equiv \frac{e\mathcal{B}(t)}{T^2(t)} = \frac{e\mathcal{B}_0}{T_0^2} \equiv b_0 = \text{ const.} \qquad 10^{-3} > b_0 > 10^{-11} , \tag{8}$$

given in natural units ($c = \hbar = k_B = 1$). We computed the bounds for this cosmic magnetic scale ratio by using the present day observations given by Eq. (1) and the present CMB temperature $T_0 = 2.7 \text{ K} \simeq 2.3 \times 10^{-4} \text{ eV}$ [23].

To evaluate paramagnetic properties of the e^-e^+ pair plasma we take inspiration from Ch. 9 of Melrose's treatise on magnetized plasmas [24]. We focus on the bulk properties of thermalized plasmas in (near) equilibrium. In considering e^+e^- pair plasma, we introduce the microscopic energy of the charged $\pm e$ relativistic fermion within a homogeneous (z-direction) magnetic field [25]. The energy eigenvalue is given by

$$E_n^\pm(p_z, \mathcal{B}) = \sqrt{m_e^2 + p_z^2 + e\mathcal{B}\left(2n + 1 \mp \frac{g}{2}\right)}, \qquad n \in 0, 1, 2, \dots \tag{9}$$

where p_z is the momentum parallel to the field axis and n is the Landau orbital quantum number. The superscript $\pm$ refers to the spin polarization along the field axis: parallel $(+)$ or anti-parallel $(-)$ for both particle and antiparticle species. The parameter g is the gyro-magnetic (g-factor) of the particle. We rearrange Eq. (9) by pulling the spin dependency and the ground state Landau orbital into the mass writing

$$E_n^\pm = \tilde{m}_\pm \sqrt{1 + \frac{p_z^2}{\tilde{m}_\pm^2} + \frac{2e\mathcal{B}n}{\tilde{m}_\pm^2}}, \qquad \tilde{m}_\pm^2 = m_e^2 + q\mathcal{B}\left(1 \mp \frac{g}{2}\right) , \tag{10}$$

where we introduced the effective polarized mass $\tilde{m}_\pm$ which is distinct for each spin alignment and is a function of magnetic field strength $\mathcal{B}$. The effective polarized mass $\tilde{m}_\pm$ allows us to describe the e^+e^- plasma with the spin effects almost wholly separated from the Landau characteristics of the gas when considering plasma thermodynamic properties.

In presence of magnetic field in Boltzmann approximation the charge neutrality condition Eq. (3) becomes

$$\sinh\frac{\mu}{T} = n_p \frac{\pi^2}{T^3} \left[\sum_s^\pm \xi_s \left(x_s^2 K_2(x_s) + \frac{b_0}{2} x_s K_1(x_s) + \frac{b_0^2}{12} K_0(x_s)\right)\right]^{-1} . \tag{11}$$

Eq. (11) is fully determined by the right-hand-side expression if the spin fugacity is set to unity $\xi = 1$ implying an equal number of polarizations both parallel and anti-parallel to the external field.

In general however, an additional physical constraint is required as the chemical μ and spin η potentials have mutual dependency. We note that such a constraint is likely related to the total angular momentum of the considered volume and does not necessarily imply that spin polarizations must be balanced within a single species when the orbital and spin momentum of all species in the plasma are taken into account.

Since our arguments addresses the temperature interval where the effects of quantum Fermi statistics on the e^+e^- pair plasma are relatively small we employ throughout the Boltzmann approximation. However, we extrapolate our results for presentation completeness up to $T \simeq 4m$. In general modifications due to quantum statistical phase space reduction for fermions are expected to reduce by about 20% such extrapolated results and perhaps by a lesser amount the relative values. We continue to search for semi-analytical solutions allowing spin ferromagnetism for Fermi statistics in relativistic e^+e^--pair abundance akin to the Boltzmann solution here offered.

We proceed now with the Boltzmann approximation for the limit where $T \lesssim m_e$. The Euler-Maclaurin formula [26] is used to convert the summation over Landau levels into an integration. The resulting partition function (after truncation

of the error remainder) can then be written in terms of modified Bessel K functions [26, 27] of the second kind, yielding

$$\ln \mathcal{Z}_{e^+e^-} \simeq \frac{T^3 V}{2\pi^2} \left[2 \cosh \frac{\mu}{T} \right] \sum_s^{\pm} \xi_s \left(x_s^2 K_2(x_s) + \frac{b_0}{2} x_s K_1(x_s) + \frac{b_0^2}{12} K_0(x_s) \right) , \tag{12}$$

$$2 \cosh \frac{\mu}{T} = \lambda + \lambda^{-1} , \qquad x_{\pm} = \frac{\tilde{m}_{\pm}}{T} = \sqrt{\frac{m_e^2}{T^2} + b_0 \left(1 \mp \frac{g}{2} \right)} . \tag{13}$$

The latter two terms in Eq. (12) (proportional to $b_0 K_1$ and $b_0^2 K_0$) are the uniquely magnetic terms present (containing both paramagnetic and diamagnetic influences) in the partition function while the K_2 term is present for the relativistic free Fermi gas [28]. As the Bessel K functions are evaluated as functions of $x_{\pm}$ in Eq. (13), the "free" part of the partition K_2 is still subject to spin magnetization effects.

4 Electron-positron magnetization

The magnetization of the e^+e^- plasma described by the partition function in Eq. (12) can be written as

$$\mathcal{M} \equiv \frac{T}{V} \frac{\partial}{\partial \mathcal{B}} \ln \mathcal{Z}_{e^+e^-} = \frac{T}{V} \left(\frac{\partial b_0}{\partial \mathcal{B}} \right) \frac{\partial}{\partial b_0} \ln \mathcal{Z}_{e^+e^-} , \qquad \frac{\partial b_0}{\partial \mathcal{B}} = \frac{q}{T^2} . \tag{14}$$

Magnetization arising from other components in the cosmic gas (protons, neutrinos, etc.) could in principle also be included. In the context of MHD, primordial magnetogenesis from neutrino interactions in the electron-positron epoch was considered in [29]. We introduce dimensionless units for magnetization by defining the critical field

$$\mathcal{B}_C \equiv \frac{m_e^2}{q} , \qquad \overline{\mathcal{M}} \equiv \frac{\mathcal{M}}{\mathcal{B}_C} . \tag{15}$$
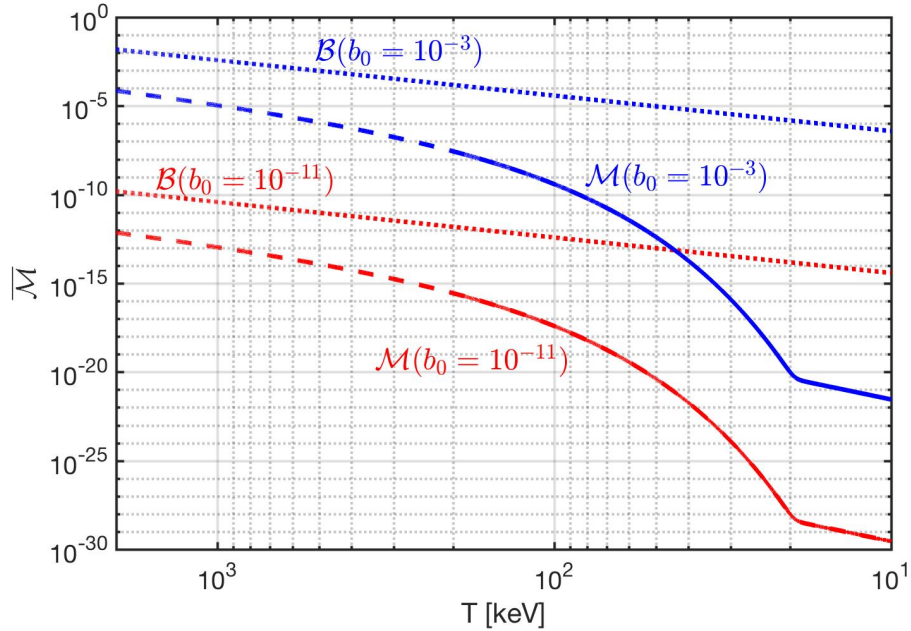

Figure 2: The magnetization $\mathcal{M}$, with $g = 2$, of the primordial e^+e^- plasma is plotted as a function of temperature. The lower (solid red) and upper (solid blue) bounds for cosmic magnetic scale b_0 are included. The external magnetic field strength $\mathcal{B}/\mathcal{B}_C$ is also plotted in for lower (dashed red) and upper (dashed blue) bounds. The spin fugacity is set to unity $\xi = 1$.

The scale $\mathcal{B}_C$ is where electromagnetism is expected to become subject to non-linear effects, though luckily in our regime of interest, electrodynamics should be linear. We note however that the upper bounds of IGMFs in Eq. (1) (with $b_0 = 10^{-3}$; see Eq. (8)) brings us to within 1% of that limit for the external field strength in the temperature
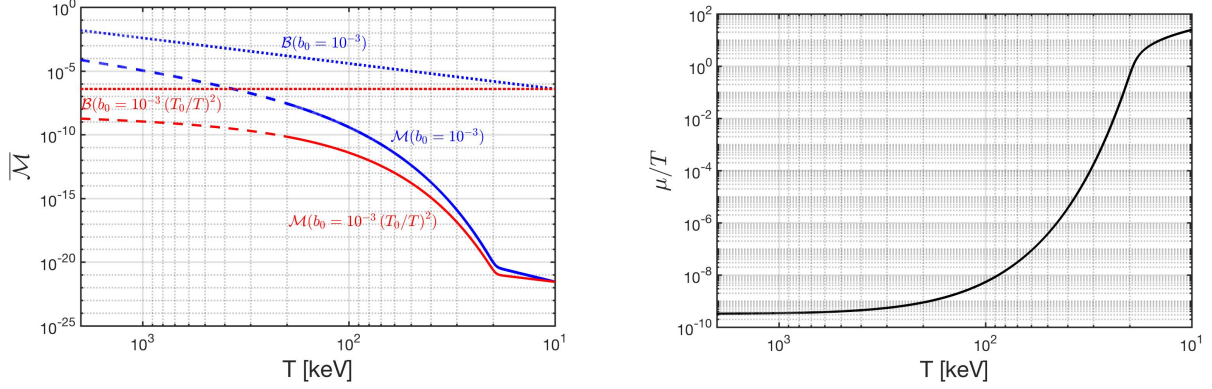
Figure 3: (left) The magnetization $\mathcal{M}$, with $g = 2$, is plotted for the $b_0 = 10^{-3}$ case (solid blue) and the constant magnetic field $b_0 = 10^{-3}(T_0/T)^2$ case (solid red) where the comoving reference temperature is $T_0 = 10$ keV. The external magnetic field strength is plotted for the conserved flux case (dashed blue) and the constant field case (dashed red). (right) The chemical potential over temperature μ/T is plotted as a function of temperature with magnetic field $b_0 = 0$ and spin potential $\eta = 0$ set to zero.

range considered. The total magnetization $\mathcal{M}$ can be broken into the sum of spin parallel $\mathcal{M}_+$ and spin anti-parallel $\mathcal{M}_-$ magnetization. We note that the expression for the magnetization simplifies significantly for $g = 2$ which is the "cusp" gyro-magnetic factor [30] for Dirac particles. For illustration, the $g = 2$ magnetization from Eq. (14) is then

$$\overline{\mathcal{M}}_+ = \frac{q^2}{\pi^2} \frac{T^2}{m_e^2} \xi \cosh \frac{\mu}{T} \left[\frac{1}{2} x_+ K_1(x_+) + \frac{b_0}{6} K_0(x_+) \right] , \qquad x_+ = \frac{m_e}{T} , \tag{16}$$

$$-\overline{\mathcal{M}}_- = \frac{q^2}{\pi^2} \frac{T^2}{m_e^2} \xi^{-1} \cosh \frac{\mu}{T} \left[\left(\frac{1}{2} + \frac{b_0^2}{12 x_-^2} \right) x_- K_1(x_-) + \frac{b_0}{3} K_0(x_-) \right] , \qquad x_- = \sqrt{\frac{m_e^2}{T^2} + 2 b_0} . \tag{17}$$

As the g-factor of the electron is only slightly above two at $g \simeq 2.00232$ [31], the above two expressions for $\overline{\mathcal{M}}_+$ and $\overline{\mathcal{M}}_-$ are only modified by a small amount because of anomalous magnetic moment (AMM). The influence of AMM would be more relevant for the magnetization of baryon gasses since the g-factor for protons ($g \approx 5.6$) and neutrons ($g \approx 3.8$) are substantially different from $g = 2$.

In Fig. 2, we plot the magnetization as given by Eq. (16) and Eq. (17) with the spin potential set to unity $\xi = 1$. We see that the e^+e^- plasma is overall paramagnetic and yields a positive overall magnetization which is contrary to the traditional assumption that matter-antimatter plasmas lack significant magnetic responses of their own in the bulk. With that said, the magnetization never exceeds the external field under the parameters considered which shows a lack of ferromagnetic behavior. As the universe cooled, the dropping magnetization slowed at $T_{\text{split}} = 20.3$ keV where positrons vanished. Thereafter the remaining electrons density n_{e^-} only diluted with cosmic expansion.

Despite the relatively large magnetization seen in Fig. 2, the average contribution per lepton is only a small fraction of its overall magnetic moment. Specifically, the magnetization regime we are in is described by

$$\mathcal{M} V \ll \mu_B (N_{e^+} + N_{e^-}) , \qquad \mu_B = \frac{q}{2m} , \tag{18}$$

where μ_B is the Bohr magneton and $N = nV$ is the total particle number in the proper volume. To better demonstrate this, we define the average magnetic moment per lepton given by along the field (z-direction) axis as

$$\langle \vec{m} \rangle_z \equiv \frac{\mathcal{M}}{n_{e^-} + n_{e^+}} , \qquad \langle \vec{m} \rangle_x = \langle \vec{m} \rangle_y = 0 . \tag{19}$$

From the spin eigen-states, we expect the transverse expectation values to be zero. The quantity given in Eq. (19) gives us an insight into the microscopic response of the plasma which we will use below.

A curious feature of Fig. 2 is that the magnetization increases as a function of temperature. This is contrary to most systems which lose their magnetization at higher temperatures because of the disordering influence of thermal heat [32]. A standard feature of paramagnetic systems (Curie's law) is that the susceptibility of the material is suppressed as temperature increases, so it is natural ask: Why doesn't this occur for the primordial e^+e^- plasma?
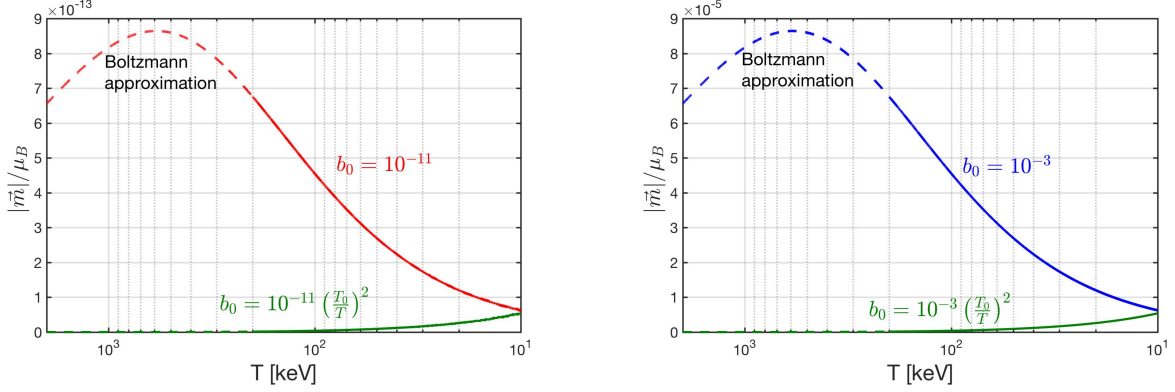
There are two reasons:

Figure 4: The magnetic moment per lepton $\langle\vec{m}\rangle_z$ along the field axis is plotted for (left) $b_0 = 10^{-11}$ and (right) $b_0 = 10^{-3}$ using the Boltzmann approximation (dashed black) and the Fermi-Dirac distribution (left: solid red; right: solid blue). Both figures display the constant magnetic field case (solid green) with the comoving value chosen at temperature $T_0 = 10$ keV.

a. As discussed in Sect. 2, the late e^+e^- plasma saw its density decrease by a factor of 10^9 as the majority of the gas annihilated leaving behind only a small residual quantity of electrons. As we travel into the distance past, the density of electrons n_{e-} and positrons n_{e+} increases by an enormous extent therefore enhancing the overall magnetization through quantity. This is shown in Fig. 3 (left) which compares the magnetization of the gas with conserved magnetic flux $b_0 = $ const and a constant field $b_0 \propto 1/T^2$. If the magnetic field is constant, we see the parameter responsible for magnetization at high temperatures is the pair density. In Fig. 3 (right) we plot the chemical potential μ/T which characterizes the importance of the charged lepton asymmetry as a function of temperature. As an aside, we only plotted the $b_0 = 0$ case as the magnetic field did not visibly influence μ/T in the regime considered.

b. The conservation of magnetic flux, as described in Eq. (7), through comoving surfaces for the external field ensures that as we travel into the past, the magnetic field increases which enhances the overall magnetization of the gas. This phenomenon is seen in Fig. 3 as the difference between the blue and red curves. However, a more striking visualization of this is plotted in Fig. 4 where the average magnetic moment $\langle\vec{m}\rangle_z$ defined in Eq. (19) displays how essential the external field is on the per lepton magnetization. The average magnetic moment per lepton is suppressed at higher temperatures (as expected for Curie law-like magnetization) if the field strength is held constant. A small difference is seen between the full Fermi distribution analysis and the Boltzmann approximation used in this work.

5 Spin potential and ferromagnetism

Up to this point, we have neglected the impact that a nonzero spin potential $\eta \neq 0$ (and thus $\xi \neq 1$) would have on the primordial e^+e^- plasma. In the limit the cosmic magnetic scale (and thus external magnetic field) goes to zero, the magnetization given in Eq. (16) and Eq. (17) is entirely controlled by the spin fugacity ξ asymmetry generated by the spin potential η yielding

$$\lim_{b_0 \to 0} \overline{\mathcal{M}} = \frac{q^2}{\pi^2} \frac{T^2}{m_e^2} \sinh\frac{\eta}{T} \cosh\frac{\mu}{T} \left[\frac{m_e}{T} K_1\left(\frac{m_e}{T}\right)\right], \qquad 2\sinh\frac{\eta}{T} = \xi - \xi^{-1}. \tag{20}$$

Therefore, we can understand the spin potential as a kind of ferromagnetic influence on the primordial gas which allows for magnetization even in the absence of external magnetic fields. As $\sinh\eta/T$ is an odd function, the sign of η also controls the alignment of the magnetization. In general, $\eta = \eta(\mu, T)$ is a function of the chemical potential and temperature. As discussed in Sect. 3, the two potentials are mutually related likely would need be simultaneously solved. We will return to the topic of spin potential constraints under separate cover.
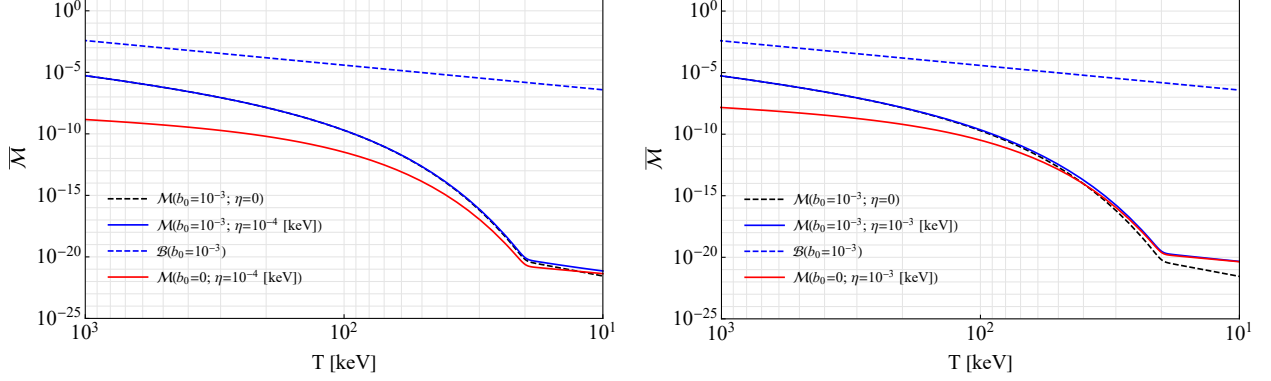
6 Closing

to be written

7

Figure 5: to be written

MOVE TO CONCLUSIONS

This combination of strong magnetic fields, high matter-antimatter density, and relatively high temperatures (far higher than the Sun's core temperature [16] of $T_\odot = 1.37$ keV) make this universe era unique in cosmology and astrophysics.

DELETE OR PLACE ELSEWHERE OR REPHRASE TO KEEP REFERENCE.

If the Cosmological Principle is correct [13], on the largest scales. Localized inhomogeneities of matter evolution are often non-trivial and generally be solved numerically using magneto-hydrodynamics (MHD) [24, 33].

References

[1] M. Giovannini. The Magnetized universe. *Int. J. Mod. Phys. D*, 13:391–502, 2004. doi:10.1142/S0218271804004530.

[2] P. P. Kronberg. Extragalactic magnetic fields. *Reports on Progress in Physics*, 57(4):325, 1994. doi:10.1088/0034-4885/57/4/001.

[3] B. M. Gaensler, R. Beck, and L. Feretti. The origin and evolution of cosmic magnetism. *New Astronomy Reviews*, 48(11-12):1003–1012, 2004. doi:10.1016/j.newar.2004.09.003.

[4] R. Durrer and A. Neronov. Cosmological magnetic fields: their generation, evolution and observation. *The Astronomy and Astrophysics Review*, 21:1–109, 2013. doi:10.1007/s00159-013-0062-7.

[5] R. A. Batista and A. Saveliev. The gamma-ray window to intergalactic magnetism. *Universe*, 7(7), 2021. ISSN 2218-1997. doi:10.3390/universe7070223.

[6] A. Neronov and I. Vovk. Evidence for strong extragalactic magnetic fields from fermi observations of tev blazars. *Science*, 328(5974):73–75, 2010. doi:10.1126/science.1184192.

[7] A. M. Taylor, I. Vovk, and A. Neronov. Extragalactic magnetic fields constraints from simultaneous gev–tev observations of blazars. *Astronomy & Astrophysics*, 529:A144, 2011. doi:10.1051/0004-6361/201116441.

[8] M. S. Pshirkov, P. G. Tinyakov, and F. R. Urban. New limits on extragalactic magnetic fields from rotation measures. *Phys. Rev. Lett.*, 116(19):191302, 2016. doi:10.1103/PhysRevLett.116.191302.

[9] K. Jedamzik and A. Saveliev. Stringent limit on primordial magnetic fields from the cosmic microwave background radiation. *Physical review letters*, 123(2):021301, 2019. doi:10.1103/PhysRevLett.123.021301.

[10] T. Vernstrom, G. Heald, F. Vazza, T. J. Galvin, J. L. West, N. Locatelli, N. Fornengo, and E. Pinetti. Discovery of magnetic fields along stacked cosmic filaments as revealed by radio and X-ray emission. *Monthly Notices of the Royal Astronomical Society*, 505(3):4178–4196, 05 2021. doi:10.1093/mnras/stab1301.

[11] V. P. Pomakov, S. P. O'Sullivan, M. Brüggen, F. Vazza, E. Carretti, G. H. Heald, C. Horellou, T. Shimwell, A. Shulevski, and T. Vernstrom. The redshift evolution of extragalactic magnetic fields. *Monthly Notices of the Royal Astronomical Society*, 515(1):256–270, September 2022. doi:10.1093/mnras/stac1805.

[12] K. Jedamzik and T. Abel. Small-scale primordial magnetic fields and anisotropies in the cosmic microwave background radiation. *JCAP*, 10:050, 2013. doi:10.1088/1475-7516/2013/10/050.

[13] E. Abdalla, G. F. Abellán, A. Aboubrahim, A. Agnello, Ö. Akarsu, Y. Akrami, G. Alestas, D. Aloni, L. Amendola, L. A. Anchordoqui, et al. Cosmology intertwined: A review of the particle physics, astrophysics, and cosmology associated with the cosmological tensions and anomalies. *Journal of High Energy Astrophysics*, 34: 49–211, 2022. doi:10.1016/j.jheap.2022.04.002.

[14] K. Jedamzik and L. Pogosian. Relieving the hubble tension with primordial magnetic fields. *Physical Review Letters*, 125(18):181302, 2020. doi:10.1103/PhysRevLett.125.181302.

[15] J. Rafelski, J. Birrell, A. Steinmetz, and C. T. Yang. A short survey of matter-antimatter evolution in the primordial universe. *MDPI Universe*, 2023. doi:10.48550/arXiv.2305.09055.

[16] J. N. Bahcall, M. H. Pinsonneault, and S. Basu. Solar models: Current epoch and time dependences, neutrinos, and helioseismological properties. *The Astrophysical Journal*, 555(2):990, jul 2001. doi:10.1086/321493.

[17] J. Birrell, C. T. Yang, and J. Rafelski. Relic Neutrino Freeze-out: Dependence on Natural Constants. *Nucl. Phys. B*, 890:481–517, 2014. doi:10.1016/j.nuclphysb.2014.11.020.

[18] M. J. Fromerth, I. Kuznetsova, L. Labun, J. Letessier, and J. Rafelski. From Quark-Gluon Universe to Neutrino Decoupling: $200 < T < 2$MeV. *Acta Phys. Polon. B*, 43(12):2261–2284, 2012. doi:10.5506/APhysPolB.43.2261.

[19] L. Canetti, M. Drewes, and M. Shaposhnikov. Matter and Antimatter in the Universe. *New J. Phys.*, 14:095012, 2012. doi:10.1088/1367-2630/14/9/095012.

[20] H. T. Elze, W. Greiner, and J. Rafelski. The relativistic Fermi gas revisited. *J. Phys. G*, 6:L149–L153, 1980. doi:10.1088/0305-4616/6/9/003.

[21] R. L. Workman et al. Review of Particle Physics. *PTEP*, 2022:083C01, 2022. doi:10.1093/ptep/ptac097.

[22] S. Weinberg. *Gravitation and cosmology: principles and applications of the general theory of relativity*. John Wiley & Sons, 1972.

[23] N. Aghanim et al. Planck 2018 results. VI. Cosmological parameters. *Astron. Astrophys.*, 641:A6, 2020. doi:10.1051/0004-6361/201833910. [Erratum: Astron.Astrophys. 652, C4 (2021)].

[24] D. Melrose. *Quantum plasmadynamics: Magnetized plasmas*. Springer, 2013. doi:10.1007/978-1-4614-4045-1.

[25] A. Steinmetz, M. Formanek, and J. Rafelski. Magnetic Dipole Moment in Relativistic Quantum Mechanics. *Eur. Phys. J. A*, 55(3):40, 2019. doi:10.1140/epja/i2019-12715-5.

[26] M. Abramowitz, I. A. Stegun, and R. H. Romer. *Handbook of mathematical functions with formulas, graphs, and mathematical tables*. American Association of Physics Teachers, 1988.

[27] J. Letessier and J. Rafelski. *Hadrons and Quark–Gluon Plasma*. Cambridge Monographs on Particle Physics, Nuclear Physics and Cosmology. Cambridge University Press, 2023. doi:10.1017/9781009290753. [Orig. pub. year: 2002].

[28] W. Greiner, L. Neise, and H. Stöcker. *Thermodynamics and statistical mechanics*. Springer Science & Business Media, 2012.

[29] L. M. Perrone, G. Gregori, B. Reville, L. O. Silva, and R. Bingham. Neutrino-electron magnetohydrodynamics in an expanding universe. *Phys. Rev. D*, 104(12):123013, 2021. doi:10.1103/PhysRevD.104.123013.

[30] J. Rafelski, S. Evans, and L. Labun. Study of QED singular properties for variable gyromagnetic ratio $g \simeq 2$. *Phys. Rev. D*, 107, 2023. doi:10.1103/PhysRevD.107.076002.

[31] E. Tiesinga, P. J. Mohr, D. B. Newell, and B. N. Taylor. Codata recommended values of the fundamental physical constants: 2018. *Journal of Physical and Chemical Reference Data*, 50(3):033105, 2021. doi:10.1063/5.0064853.

[32] K. Huang. *Statistical Mechanics*. Wiley, 1991. 2nd Ed.

[33] F. Vazza, M. Brüggen, C. Gheller, S. Hackstein, D. Wittor, and P. M. Hinz. Simulations of extragalactic magnetic fields and of their observables. *Class. Quant. Grav.*, 34(23):234001, 2017. doi:10.1088/1361-6382/aa8e60.